

# A sagging-spreading continuum of large volcano structure

P.K. Byrne<sup>1,4</sup>, E.P. Holohan<sup>2</sup>, M. Kervyn<sup>3</sup>, B. van Wyk de Vries<sup>4</sup>, V.R. Troll<sup>5</sup>, and J.B. Murray<sup>6</sup>

<sup>1</sup>Department of Terrestrial Magnetism, Carnegie Institution of Washington, 5241 Broad Branch Road NW, Washington, D.C. 20015, USA

<sup>2</sup>School of Geological Sciences, University College Dublin, Belfield, Dublin 4, Ireland

<sup>3</sup>Department of Geography, Vrije Universiteit Brussels, Pleinlaan 2 050 Brussels, Belgium

<sup>4</sup>Laboratoire Magmas et Volcans, Université Blaise-Pascal, 5 Rue Kessler, 63038 Clermont-Ferrand Cedex, France

<sup>5</sup>Department of Earth Sciences, Uppsala University, Villavägen 16 B, 751 05 Uppsala, Sweden

<sup>6</sup>Department of Earth and Environmental Sciences, The Open University, Walton Hall, Milton Keynes MK7 6AA, UK

## ABSTRACT

**Gravitational deformation strongly influences the structure and eruptive behavior of large volcanoes. Using scaled analog models, we characterize a range of structural architectures produced by volcano sagging and volcano spreading. These arise from the interplay of variable basement rigidity and volcano-basement (de-)coupling. From comparison to volcanoes on Earth (La Réunion and Hawaii) and Mars (Elysium and Olympus Mons), the models highlight a structural continuum in which large volcanoes throughout the Solar System lie.**

## INTRODUCTION

Understanding a volcano's structural development is crucial for studies of volcanic hazard, eruption behavior, and lithospheric dynamics. Volcano sagging and spreading are two gravity-driven deformation processes that shape large volcanoes on terrestrial planets over  $10^1$ – $10^6$  yr. Volcano spreading occurs when the lateral weight gradient of an edifice causes its slow outward collapse along a basal décollement (Borgia et al., 2000). Sagging results when a volcano's weight down-flexes its underlying basement and lithosphere (e.g., Zucca et al., 1982).

Structures related to volcano spreading are well understood (cf. Borgia et al., 2000): folds and thrusts occur at or beyond the edifice's base, while normal faults and "leaf grabens" crosscut its flanks (Fig. 1A). Structures formed by volcano sagging are less understood, but include an edifice-encircling trough, peripheral joints of grabens, a flexural bulge (e.g., Kervyn et al., 2010), and possibly enigmatic "flank terraces" on the edifice itself (Byrne et al., 2009) (Fig. 1B).

Volcano sagging and spreading may interact, as at Olympus Mons (Fig. 1C) and Hawaii (United States; Fig. 1D), the largest volcanoes on Mars and Earth, respectively. Both exhibit normal faults and grabens on their mid- to lower flanks, and either a prominent scarp or a fold-and-thrust belt linked to thrusting along a major décollement at their bases (Lopes et al., 1980; Thurber and Gripp, 1988). They also display terraces on their mid- to upper flanks (Byrne et al., 2009), and flexural troughs and bulges in their surrounding basements (Dietz and Menard, 1953; McGovern et al., 2002).

Yet the conditions, timing, and structural outcomes of such interaction remain unclear. Most past modeling efforts considered only one process (e.g., McGovern and Morgan, 2009), while those including both (e.g., van Wyk de Vries and Matela, 1998) used continuum-based numerical approaches that did not directly simulate discontinuous deformation (i.e., faulting). To address

the combined structural development of both processes, we ran a set of scaled analog models.

## ANALOG MODEL SETUP AND SCALING

All models occupied a large cylindrical container, into which we placed a lower layer of

silicone putty and an upper layer of sand-gypsum mix, corresponding to the ductile (aseismic) and brittle (seismogenic) parts of the lithosphere, respectively (Watts and Burov, 2003) (Figs. 2A and 2B). A sand-gypsum cone, representing a volcanic edifice, was built upon the basement. A thin (<1 mm) layer of pure gypsum was added to the surface to help preserve small-scale structures.

To some models, we added a thin silicone layer just below the cone's base (Fig. 2C). The spatial extent of this layer was set to either slightly less, or significantly greater, than the cone diameter. This layer represented a décollement localized

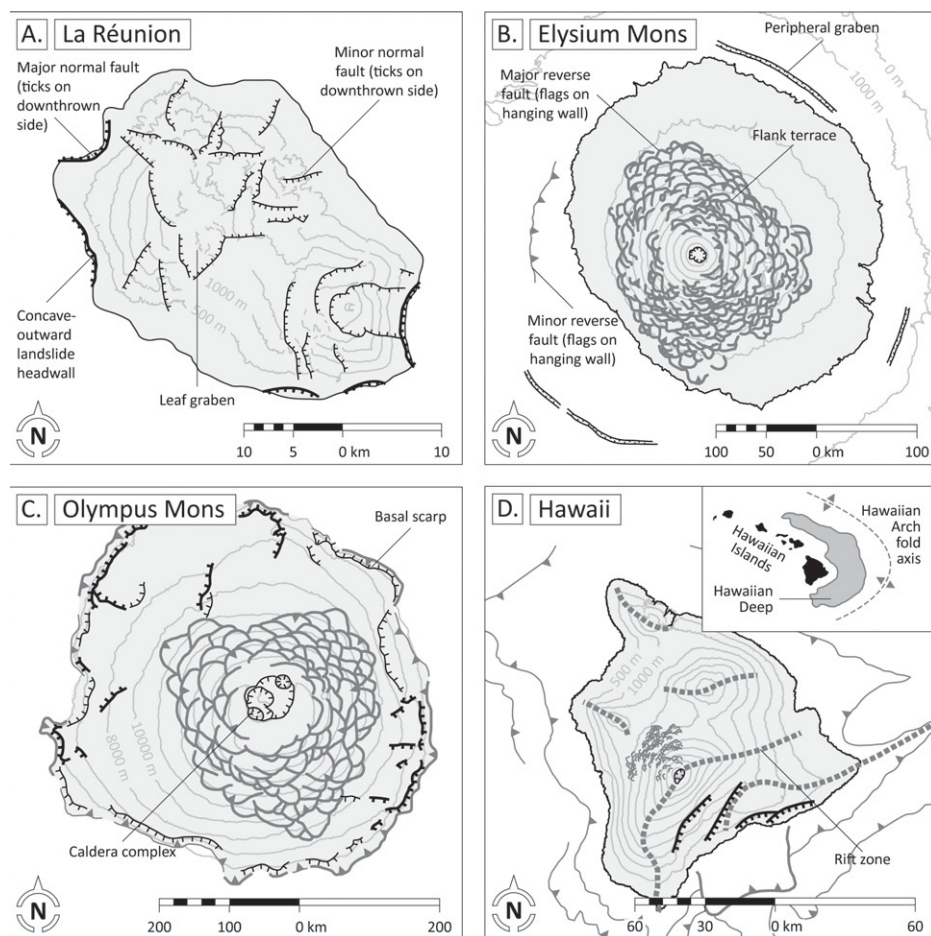


**Figure 1. Structural sketches of gravitationally deformed volcanoes. A: La Réunion, Earth. B: Elysium Mons, Mars, after Byrne et al. (2009). C: Olympus Mons, Mars, modified from Byrne et al. (2009) and McGovern and Morgan (2009). D: The Big Island of Hawaii, based on U.S. Geological Survey DEM data. Inset shows a flexural trough (the Hawaiian Deep, shaded) and a surrounding bulge (the Hawaiian Arch, axis dashed), after Dietz and Menard (1953).**

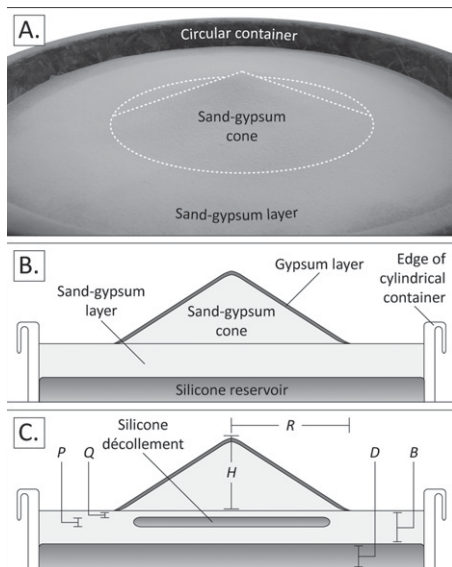


**Figure 2. Experimental setups. A: Setup for a cone coupled to its basement (cone outline dashed in white). B: Schematic cross section of this setup. C: Cross section of the decoupled cone setup.**

within incompetent materials, such as altered or water-saturated rock, poorly consolidated volcanoclastics, or ice-rich regolith (cf. Tanaka, 1985; McGovern and Morgan, 2009). We did not model changes in basement or décollement viscosity, or intrusions within the cone, which can further affect deformation rate and style (Borgia, 1994; van Wyk de Vries and Matela, 1998). Model horizontal displacements and strains were quantified by particle image velocimetry (PIV) analysis of time-lapse photos in the software DaVis (cf. Walter, 2011).

Model scaling, and its applicability to nature, are detailed in the GSA Data Repository<sup>1</sup>. We define two dimensionless parameters that control sagging ( $\Pi_{\text{Sag}}$ ) or spreading ( $\Pi_{\text{Spread}}$ ).  $\Pi_{\text{Sag}}$  relates the cone gravitational load and geometry to the effective flexural rigidity of the basement, and is defined as

$$\Pi_{\text{Sag}} = \frac{(4.11 \times \rho \times g \times R^2 \times H^2)(1 - \nu^2)}{(E \times B^3)} \quad (1)$$

This equation incorporates cone height ( $H$ ), cone radius ( $R$ ), brittle-lithosphere thickness ( $B$ ), density ( $\rho$ ), gravitational acceleration ( $g$ ), Young's modulus ( $E$ ), and Poisson's ratio ( $\nu$ ).  $\Pi_{\text{Spread}}$  relates the gravitational potential of the cone to the configuration of the décollement and

is defined in terms of resistance to spreading (after Merle and Borgia, 1996) by

$$\Pi_{\text{Spread}} = Q^2 / (H \times P), \quad (2)$$

where  $Q$  is décollement depth and  $P$  is décollement thickness.

Within  $\Pi_{\text{Sag}}$  and  $\Pi_{\text{Spread}}$ , we varied only  $B$  and  $P$ . From the cubic scaling in Equation 1, varying  $B$  from 1 to 7 cm increases the experimental basement rigidity by a factor of >300, regulating sagging. For  $P = 0$  (cone coupled to basement),  $\Pi_{\text{Spread}} = \infty$  and spreading is impossible. For  $P = 0.5$  cm (cone decoupled from basement),  $\Pi_{\text{Spread}} = 2.5 \times 10^{-2}$  and spreading is strongly promoted (occurring in theory at  $\Pi_{\text{Spread}} < \sim 0.17$  and experimentally at  $\Pi_{\text{Spread}} < 0.6 \pm 0.5$ ; cf. Borgia et al., 2000).

## MODEL RESULTS

### Models Without a Basal Décollement

(i.e.,  $\Pi_{\text{Spread}} = \infty$ )

With  $2.4 > \Pi_{\text{Sag}} > 0.017$ , the cone subsided within a trough encompassed by a bulge (Fig. 3A). Peripheral horizontal extension formed a network of fissures and normal faults. Outside this network, horizontal displacements were directed radially outward; inside, they were directed radially inward, with magnitudes decreasing toward the cone's summit. Central horizontal contraction reduced the cone's basal diameter and localized upon a "fish scale" pattern of imbricate, outward-verging convexities on its mid- to lower flanks. With  $\Pi_{\text{Sag}} < 0.017$ , the trough shallowed and the bulge migrated outward. Horizontal displacements, central contraction, and peripheral extension diminished. At  $\Pi_{\text{Sag}} \approx 0.008$ , the basement and cone remained undeformed.

### Models with a Basal Décollement

(i.e.,  $\Pi_{\text{Spread}} = 2.5 \times 10^{-2}$ )

For a décollement "restricted" to within the cone's diameter, and with  $2.4 > \Pi_{\text{Sag}} > \sim 0.033$ , a large monoclinial fold or escarpment formed around the cone's base (Fig. 3B). Horizontal displacement magnitudes decreased abruptly inside this basal scarp, and a large contraction along the discontinuity marked it as a major thrust fault trace.

For  $\sim 0.033 > \Pi_{\text{Sag}} > 0.017$ , sagging diminished and the cone diameter increased as deformation progressed (Fig. 3C). Outward horizontal displacement, with extension on fissures and normal faults, began to characterize the cone's lower flanks. Inward displacement, with associated contraction and convexities, shifted to the upper flanks. Greater relative motion between the cone and the basement yielded a steeper and more pronounced basal scarp, the leading edge of which collapsed in places (Fig. 3B versus Fig. 3C).

For  $0.017 > \Pi_{\text{Sag}} > \sim 0.008$ , sagging ceased soon after loading, and spreading dominated thereafter (Fig. 3D). Although initially inward-directed, horizontal displacements became outward-directed overall. The cone's basal diameter increased, and its flanks underwent extension along near-radial normal faults delimiting leaf grabens. The basal scarp was more pronounced, oversteepened, and unstable. At  $\Pi_{\text{Sag}} \approx 0.008$ , the basement remained essentially undeformed, and the outward-spreading cone underwent extension from its lowermost flanks to its summit. For an "unrestricted" detachment extending beyond the cone's diameter, a distributed fold-and-thrust belt developed around the cone's base (see Fig. DR1 in the Data Repository).

## DISCUSSION

Our experiments show that a continuum of volcano structural architectures arises from the interplay of (1) the effective rigidity and strength of a basement with respect to a volcanic load, and (2) the effective coupling or decoupling of the load from its basement.

### Model Kinematics

End-member sagging architectures (Fig. 3A) result when a cone and its flexible basement are coupled and deform as one mechanical unit. Outer-arc extension next to the flexural bulge produces peripheral fissures and normal faults. Inner-arc contraction in the flexural trough decreases the cone's basal diameter and forms a system of terrace-like convexities (imbricate thrusts with hanging-wall anticlines) on the cone's flanks (Fig. 4A).

Hybrid sagging-spreading architectures result when a cone and its flexible basement are decoupled and deform as two discrete units (Fig. 3B). When sagging is pronounced and active ( $\Pi_{\text{Sag}} > \sim 0.033$ ), differential motion between the units occurs along the décollement and maintains the cone's diameter. This apparent flexural slip produces a large thrust fault scarp around the cone's base. Inner-arc contraction of the cone's mid- to upper flanks forms terraces there, while outer-arc extension of the cone's base leads to tensile fractures and normal faults on its lower flanks (Fig. 4B). When sagging is weak ( $\Pi_{\text{Sag}} \leq \sim 0.033$ ), the buttressing effect of the trough diminishes; spreading increasingly drives slip on the décollement, shown as an increase of the cone's diameter after initial sagging ends (Fig. 3C). Dominance of spreading over sagging promotes near-radial normal faulting on the decoupled cone's mid- to lower flanks.

End-member spreading architectures, dominated by normal faults and leaf grabens (Fig. 3D), result when a decoupled cone collapses outward across a rigid and essentially undeformed basement (Fig. 4C).

Our analog structures agree well with stress patterns in continuum-based numerical models

<sup>1</sup>GSA Data Repository item 2013090, model scaling parameters, dimensionless numbers analysis, and unrestricted décollement model results, is available online at [www.geosociety.org/pubs/ft2013.htm](http://www.geosociety.org/pubs/ft2013.htm), or on request from [editing@geosociety.org](mailto:editing@geosociety.org) or Documents Secretary, GSA, P.O. Box 9140, Boulder, CO 80301, USA.

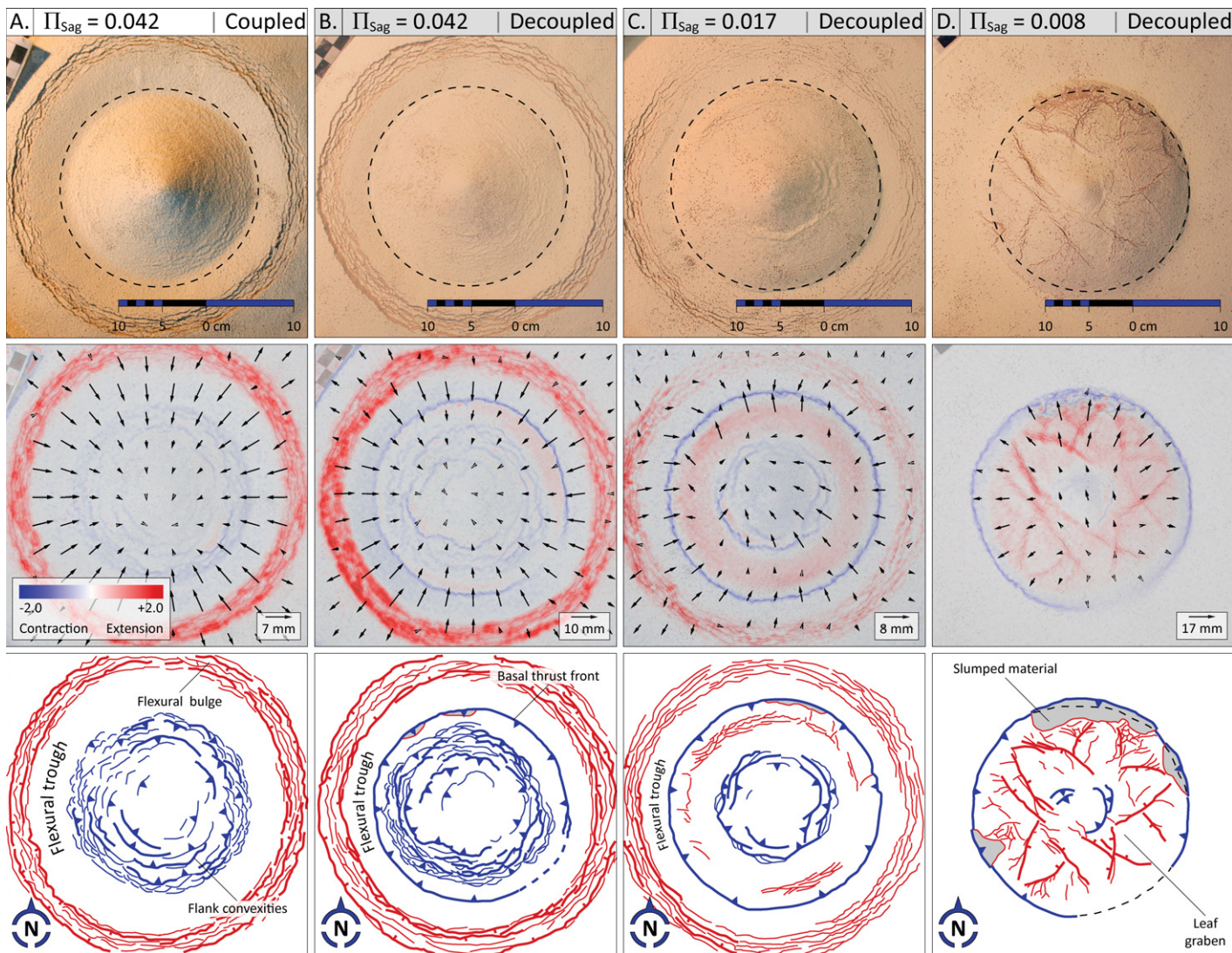


**Figure 3. Experimental results.** Top row: Plan-view photographs of deformation (dashed circle shows the initial cone diameter). Middle row: Cumulative horizontal displacements and strain fields (dilatation [or area change] =  $E_{xx} + E_{yy}$ ). Bottom row: Structural sketches. Thick or thin lines are major or minor faults; red are normal (ticks on the downthrown side); blue are reverse (flags on the hanging wall). A: Basement-coupled cone ( $\Pi_{\text{Sag}} = 0.042$ ). B–D: Decoupled cones ( $\Pi_{\text{Sag}} = 0.042, 0.017, \text{ and } 0.007$ , respectively).

of (1) volcano-induced flexure, (2) flexure with aspects of spreading along a ductile or low-friction detachment, and (3) pure volcano spreading (cf. McGovern and Solomon, 1993; Borgia, 1994; van Wyk de Vries and Matela, 1998). While our models did not simulate incremental volcano growth, numerical models that did (e.g., McGovern and Solomon, 1993) suggest lower stress magnitudes but similar structural arrangements. Such agreement supports the broad applicability of our results.

### Natural Examples

The model end-member sagging architecture closely matches that of Elysium Mons (Fig. 1B) and other Martian volcanoes (Byrne et al., 2009). These volcanoes therefore lack an effective basal decoupling, and as also suggested by correlated gravity and topographic data (McGovern et al., 2002), they overlie thin

(and thus flexible) basements relative to the edifice load. Our results support the interpretation of flank terraces as caused by lithospheric flexure (Byrne et al., 2009).

The hybrid sagging-spreading architecture of Olympus Mons, with its mid- to upper flank terraces and its lower-flank normal faults (Fig. 1C), can be explained by decoupling of the volcano from a flexing basement. Its distinctive 6–8-km-high basal scarp can be attributed to mass wasting along a thrust front formed largely by flexural slip. Our models therefore illustrate the importance of not only spreading (Borgia et al., 2000; McGovern and Morgan, 2009), but also sagging, in this volcano's structural development.

On Earth, geophysical data enable estimates of  $\Pi_{\text{Sag}}$  (see the Data Repository). For Hawaii,  $\Pi_{\text{Sag}} \approx 0.025\text{--}0.074$ , which in experiments leads to a dominance of sagging. This is consistent with geophysical and bathymetric evidence for

lithospheric flexure of 7–8 km (Dietz and Menard, 1953; Zucca et al., 1982), though less so with the restricted, subtle terracing of Mauna Loa's northwest flank and the dominance of spreading features on the Big Island's upper and lower slopes (Fig. 1D). Additional mechanisms that enhance edifice spreading, such as magmatic intrusions (Borgia, 1994) or elevated pore fluid pressure, may thus play an important role at Hawaii. For La Réunion, conversely,  $\Pi_{\text{Sag}} \approx 0.006\text{--}0.016$ , which experimentally leads to a dominance of spreading with only very subtle sagging. This is consistent with geophysical and structural observations (Fig. 1A) (e.g., Gallart et al., 1999).

More generally, our results help inform studies of volcanic hazard, eruption behavior, and lithosphere dynamics. The models show that sagging decreases, while spreading increases, the risk of landslide and sector collapse (Fig. 3).

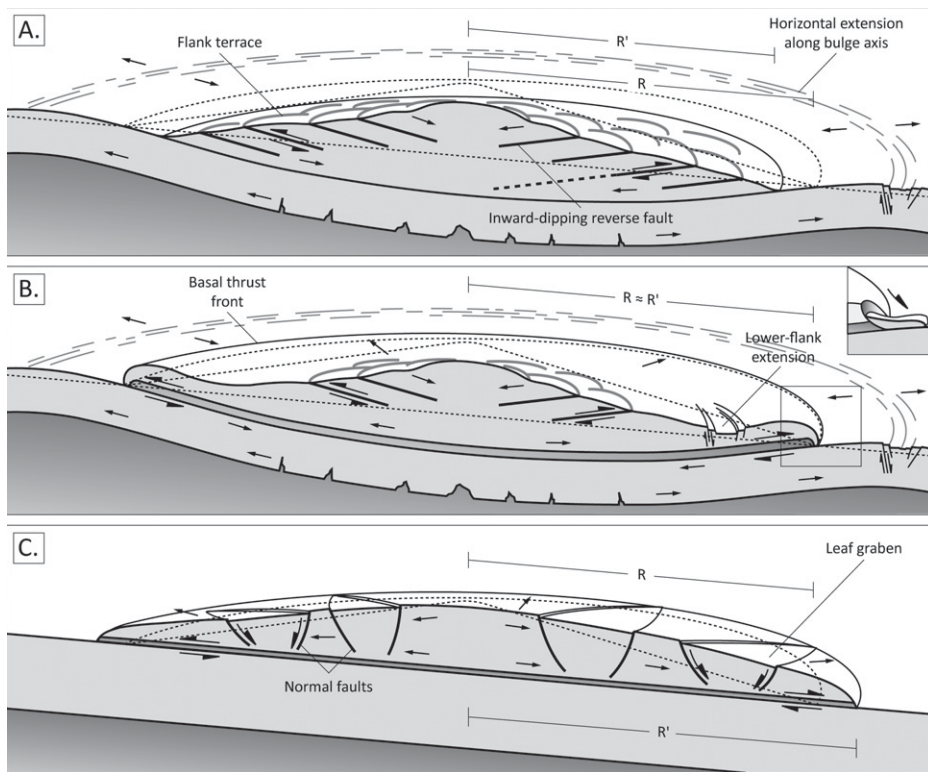


**Figure 4. Schematic block diagrams of the continuum of large volcano structure. Dotted lines show predeformed states. Small arrows indicate movement directions; half-arrow pairs indicate the slip sense on faults.  $R$ —initial cone diameter;  $R'$ —final cone diameter. A: End-member sagging architecture. B: Hybrid sagging-spreading architecture. Inset shows how material may collapse due to oversteepening of the prominent basal thrust scarp. C: End-member spreading architecture.**

They allow evaluation of likely sagging- or spreading-influenced sites of intrusive and eruptive activity (cf. Kervyn et al., 2009; Delcamp et al., 2012a, 2012b). They also enable recognition of mechanical interaction of volcano and basement during flexure, a factor rarely considered in estimates of lithosphere properties such as elastic thickness. Finally, our experiments provide a basis for better understanding geodetically measured volcano deformation, from which further modeling of natural complexities (e.g., dike/sill intrusions, incremental volcano growth, and varying deformation rates) could be considered.

In summary, our models isolate structural architectures of volcano sagging and volcano spreading end members, and characterize a continuum between them. We show that a volcano's position within this continuum depends on edifice-basement coupling and on the basement's flexural properties. This provides a first-order framework for understanding the role of gravity-driven deformation in the structural and eruptive development of large volcanoes throughout the Solar System.

#### ACKNOWLEDGMENTS

Byrne, Holohan, and Kervyn contributed equally to this study. J. Dohm, J.J. Walsh, T. Walter, and C. Wolfe gave helpful advice; P. McGovern and A. Mannoni provided thoughtful reviews. Byrne and Troll acknowledge funding from Trinity College, Dublin,

Ireland, and the Enterprise Ireland International Collaboration program (grant no. IC/2006/37/MEV-1). Holohan acknowledges an INSPIRE International Mobility Fellowship co-funded by Marie Curie Actions and the Irish Research Council (IRCSET).

#### REFERENCES CITED

- Borgia, A., 1994, Dynamic basis of volcanic spreading: *Journal of Geophysical Research*, v. 99, p. 17,791–17,804, doi:10.1029/94JB00578.
- Borgia, A., Delaney, P., and Denlinger, R., 2000, Spreading volcanoes: *Annual Review of Earth and Planetary Sciences*, v. 28, p. 539–570, doi:10.1146/annurev.earth.28.1.539.
- Byrne, P., van Wyk de Vries, B., Murray, J., and Troll, V., 2009, The geometry of volcano flank terraces on Mars: *Earth and Planetary Science Letters*, v. 281, p. 1–13, doi:10.1016/j.epsl.2009.01.043.
- Delcamp, A., van Wyk de Vries, B., James, M., Gailler, L., and Lebas, E., 2012a, Relationships between volcano gravitational spreading and magma intrusion: *Bulletin of Volcanology*, v. 74, p. 743–765, doi:10.1007/s00445-011-0558-9.
- Delcamp, A., Troll, V., van Wyk de Vries, B., Carracedo, J., Petronis, M., Pérez-Torrado, F., and Deegan, F., 2012b, Dykes and structures of the NE rift of Tenerife, Canary Islands: A record of stabilisation and destabilisation of ocean island rift zones: *Bulletin of Volcanology*, v. 74, p. 963–980, doi:10.1007/s00445-012-0577-1.
- Dietz, R., and Menard, H., 1953, Hawaiian Swell, Deep, and Arch, and subsidence of the Hawaiian Islands: *Journal of Geology*, v. 61, p. 99–113, doi:10.1086/626059.
- Gallart, J., Driad, L., Charvis, P., Sapin, M., Hirn, A., Diaz, J., de Voogd, B., and Sachpazi, M.,

- 1999, Perturbation to the lithosphere along the hotspot track of La Réunion from an offshore-onshore seismic transect: *Journal of Geophysical Research*, v. 104, p. 2895–2908.
- Kervyn, M., Ernst, G., van Wyk de Vries, B., Mathieu, L., and Jacobs, P., 2009, Volcano load control on dyke propagation and vent distribution: Insights from analogue modeling: *Journal of Geophysical Research*, v. 114, B03401.
- Kervyn, M., Boone, M., van Wyk de Vries, B., Lebas, E., Cnudde, V., Fontijn, K., and Jacobs, P., 2010, 3D imaging of volcano gravitational deformation by computerized X-ray microtomography: *Geosphere*, v. 6, p. 482–498, doi:10.1130/GES00564.1.
- Lopes, R., Guest, J., and Wilson, C., 1980, Origin of the Olympus Mons aureole and perimeter scarp: *Earth, Moon, and Planets*, v. 22, p. 221–234, doi:10.1007/BF00898433.
- McGovern, P., and Morgan, J., 2009, Volcanic spreading and lateral variations in the structure of Olympus Mons, Mars: *Geology*, v. 37, p. 139–142, doi:10.1130/G25180A.1.
- McGovern, P., and Solomon, S., 1993, State of stress, faulting, and eruption characteristics of large volcanoes on Mars: *Journal of Geophysical Research*, v. 98, p. 23,553–23,579, doi:10.1029/93JE03093.
- McGovern, P., Solomon, S., Smith, D., Zuber, M., Simons, M., Wiczorek, M., Phillips, R., Neumann, G., Aharonson, O., and Head, J., 2002, Localized gravity/topography admittance and correlation spectra on Mars: Implications for regional and global evolution: *Journal of Geophysical Research*, v. 107, p. 1–25.
- Merle, O., and Borgia, A., 1996, Scaled experiments of volcanic spreading: *Journal of Geophysical Research*, v. 101, p. 13,805–13,817, doi:10.1029/95JB03736.
- Tanaka, K., 1985, Ice-lubricated gravity spreading of the Olympus Mons aureole deposits: *Icarus*, v. 62, p. 191–206, doi:10.1016/0019-1035(85)90117-4.
- Thurber, C., and Gripp, A., 1988, Flexure and seismicity beneath the south flank of Kilauea volcano and tectonic implications: *Journal of Geophysical Research*, v. 93, p. 4271–4278, doi:10.1029/JB093iB05p04271.
- van Wyk de Vries, B., and Matela, R., 1998, Styles of volcano-induced deformation: Numerical models of substratum flexure, spreading and extrusion: *Journal of Volcanology and Geothermal Research*, v. 81, p. 1–18, doi:10.1016/S0377-0273(97)00076-0.
- Walter, T.R., 2011, Structural architecture of the 1980 Mount St. Helens collapse: An analysis of the Rosenquist photo sequence using digital image correlation: *Geology*, v. 39, p. 767–770, doi:10.1130/G32198.1.
- Watts, A., and Burov, E., 2003, Lithospheric strength and its relationship to the elastic and seismogenic layer thickness: *Earth and Planetary Science Letters*, v. 213, p. 113–131, doi:10.1016/S0012-821X(03)00289-9.
- Zucca, J., Hill, D., and Kovach, R., 1982, Crustal structure of Mauna Loa volcano, Hawaii, from seismic refraction and gravity data: *Bulletin of the Seismological Society of America*, v. 72, p. 1535–1550.

Manuscript received 28 August 2012

Revised manuscript received 21 September 2012

Manuscript accepted 25 September 2012

Printed in USA